Journal of Membrane Science 320 (2008) 173–178

Contents lists available at ScienceDirect

Journal of Membrane Science

journal homepage: www.elsevier.com/locate/memsci

Comparing flat and micro-patterned surfaces: Gas permeation and tensile stress measurements

Alisia M. Peters, Rob G.H. Lammertink*, Matthias Wessling

Membrane Technology Group, Mesa+ Institute for Nanotechnology, University of Twente, P.O. Box 217, 7500 AE Enschede, The Netherlands

ARTICLE INFO

Article history:
Received 31 January 2008
Received in revised form 27 March 2008
Accepted 28 March 2008
Available online 8 April 2008

Keywords:
Membrane
Micro-patterning
Gas permeability
Tensile stress
Simulations

ABSTRACT

Micro-patterning is a suitable method to produce structured membranes that display increased flux compared to flat membranes. In this work we studied the permeation of four different gases (nitrogen, helium, oxygen and carbon dioxide) through Kraton™ polymer (SBS) membranes. It is possible to cast a micro-patterned membrane with 25 μm high and 30 μm wide lines that has a thickness of 5 μm at its thinnest point. Using this micro-pattern, the experimental diffusive gas flux was increased up to 59% compared to non-patterned membranes with the same polymer volume. Finite element simulations confirm this enhancement. Selectivities are similar for both flat and micro-patterned membranes and in accordance with literature. Tensile stress measurements confirm that the micro-patterned membranes yield only limited loss in mechanical strength. Although only one material and geometry is explored here, this principle is generally applicable to all diffusion-driven processes.

1. Introduction

Selectivity and permeability are material properties that characterize the membrane performance. By adapting the geometry of a membrane the flux can be improved without loss in selectivity. Thinner films lead to higher fluxes, but also a lower mechanical strength. This problem is overcome by creating composite membranes. The membrane is coated as a very thin layer onto a support which provides the mechanical strength [1].

Another possibility to increase flux is to increase the effective membrane surface. Gronda et al. [2] used a double mold to create macrocorrugations (mm range) on both sides. Although theory predicts a fivefold flux increase for pervaporation, the maximal experimental increase was twofold. For high permeable solutes there was no increase observed at all due to depletion of the solute at the surface. It was also stated that macrocorrugated membranes do not have a future in industrial applications, because they are too large to fit into industrial modules. Theory, however, predicts that smaller geometries (nanocorrugated membranes) could also yield similar enhancements.

Nijdam et al. [3] demonstrated a method to increase the flux through a hollow fiber by changing its geometry. The outer surface area of the hollow fiber was increased by 19% due to patterning using a spinneret insert. Gas permeation measurements proved that the membrane properties such as the selectivity, normalized permeability and skin thickness were comparable to the circular fibers. Not only the outer surface, but also the inner surface could be micro-patterned.

These researchers have shown us that patterning a surface can be advantageous in terms of enhancing flux while maintaining selectivity. However, surface enhancement is not the only mechanism playing a role. By reshaping a given amount of polymer as a micro-pattern the diffusion paths through the membrane are altered. Its flux increases compared to a flat membrane with the same amount of polymer. This mechanism is presented in this paper by comparing patterned and non-patterned dense membranes for gas permeation. The research is also extended to composite membranes by comparing a fully permeable micro-patterned membrane with a partly non-permeable membrane (composite) of the same geometry.

2. Experimental

All materials were used as received. The block copolymer Kraton™ D-1102CS (styrene–butadiene–styrene, Kraton™ polymers) was dissolved in toluene (Merck, analysis grade) to make 30 wt% solutions. This polymer is linear containing 29.5 wt% styrene, which results in a cylindrical morphology on the nanoscale. These materials were chosen to ensure easy release of thin films from silicon wafers.

* Corresponding author. Tel.: +31 53 4892950; fax: +31 53 4894611.
E-mail address: r.g.h.lammertink@utwente.nl (R.G.H. Lammertink).

0376-7388/$ – see front matter © 2008 Elsevier B.V. All rights reserved.
doi:10.1016/j.memsci.2008.03.052

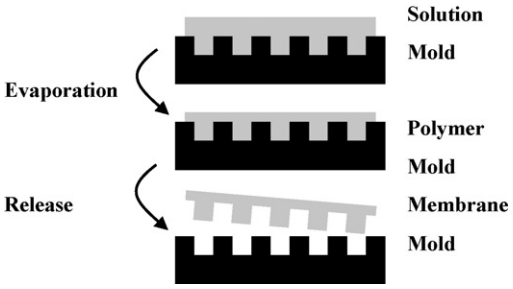

Fig. 1. Schematic representation of the membrane micro-patterning method (side view).

2.1. Membrane preparation

Dense flat sheet membranes are obtained by casting a polymer solution on a substrate [4] and removing the film after evaporation of the solvent (Fig. 1). The substrate is either a flat 4-in. silicon wafer or a silicon mold with a line pattern. The mold was produced in a clean room by standard photolithography, followed by deep reactive ion etching. The dimensions of the structures on the mold are: depth of channel = 25 μm, width of channel = 30 μm, width between channels = 20 μm. The evaporation occurred overnight and the membrane was released by using ethanol and gentle pulling. The membrane was then dried overnight in a vacuum oven at 303 K. The result is a continuous polymer film with ridges (25 μm high and 30 μm wide), a perfect replica of the mold-pattern. The thickness of the continuous film can easily be varied by changing the casting thickness.

2.2. SEM

A JEOL 5600 scanning electron microscope (SEM) was used to determine the structure and thickness of the membranes. The membranes were broken in liquid nitrogen and sputtered with a 30 nm gold layer (Balzers Union SCD 040). Pictures were taken at 5 kV.

2.3. Gas permeation

Gas permeation measurements were done in a home-built low-pressure set-up with a permeation area of 11.95 cm^2/cell [5]. The measurements are performed at a constant volume and variable pressure. The four gases nitrogen, helium, oxygen and carbon dioxide were always measured in the same order. The applied pressure was 2.5 bar on the feed side and initial vacuum on the permeate side. During measurements the permeate gas was collected. The operating temperature was 308 K. The micro-patterned side of the membranes faced the feed side. The orientation of the pattern is important as the pattern will be deformed when pressed against the membrane support when it is facing the permeate side.

2.4. Tensile stress

The tensile stress was calculated from measurements with a tensiometer (Zwick Z020). The ISO37 standard was used for sample preparation. The preload was set at 0.05 N. The membranes were stretched at a velocity of 10 mm/min. The force to reach a certain strain was measured and the effective membrane thickness was used to calculate the average stress within the whole membrane. The tensile stress was evaluated at 5% strain to compare each membrane equally. Their effective thicknesses vary from 13.5 to 47.7 μm. Hysteresis measurements have revealed that 5% strain is within the elastic regime for these membranes.

2.5. Simulations

Gas permeation simulations were performed based on a finite element method in the convection and diffusion module of COMSOL Multiphysics 3.3. The micro-patterned membrane was represented by a 25 μm wide cross-section containing half of the ridge and half of the continuous film. The vertical walls can be regarded as symmetry boundaries. The thickness of the continuous film was varied to simulate different effective membrane thicknesses. The calculations were simplified by assuming isotropic diffusion without convection. At the feed side an initial gas concentration $c_0 = 4\,mol/m^3$ and at the permeate side a vacuum ($c_0 = 0\,mol/m^3$) was applied. All other boundaries were assumed insulating/symmetrical. The diffusion coefficient D was set at $2.8 \times 10^{-11}\,m^2/s$, the experimentally determined value for nitrogen permeation. These values were used in all simulations as the final enhancement results are independent of the concentration gradient and diffusion constant. To verify this, the constants were varied up to two orders of magnitude. The mesh size was decreased until the result was constant. A typical mesh size is 10^{-7} m. A stationary nonlinear direct (UMFPACK) solver was used. The diffusive flux was determined by integrating over the permeate boundary of the membrane.

3. Results and discussion

3.1. Membrane preparation

Micro-patterned and flat membranes of equal volume are compared. Fig. 2 shows that a micro-patterned membrane with a continuous layer of 15 μm and 25 μm high ridges is comparable to a flat membrane with an effective membrane thickness (Δx) of 30 μm.

If a flat dense membrane is too thin (<30 μm), it is very difficult to remove it from a wafer without rupturing the film. Micro-patterning membranes, however, can create much thinner sections, while maintaining sufficient mechanical strength. Fig. 3 shows SEM pictures of two micro-patterned membranes, one with a relatively thick continuous film of ~50 μm (A) and one with a thinner continuous film of ~5 μm (B). The waviness of this membrane is due to the shrinkage during drying on the mold. There is a solvent concentration gradient towards the mold substrate during evaporation. When the thin continuous film is mostly dried, the membrane ridges still contain solvent. Further evaporation of solvent from these ridges results in further shrinkage and a deformation of the continuous film.

3.2. Gas permeation

Gas permeation experiments on flat and micro-patterned films were performed and compared with analytical calculations and finite element simulations. Eqs. (1) and (2) show the one-dimensional flux-equations (for this particular line pattern) based on Fick's first law of diffusion [6]. This approach neglects any lateral diffusion in the membrane. It can be used to quickly estimate the advantage of micro-patterning. For the micro-patterned membrane, the flux-equation is divided into two parts: the flux

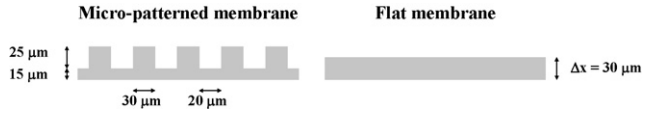

Fig. 2. Schematic representation of the cross-section of a micro-patterned membrane (left) and a flat membrane (right) with the same polymer volume.

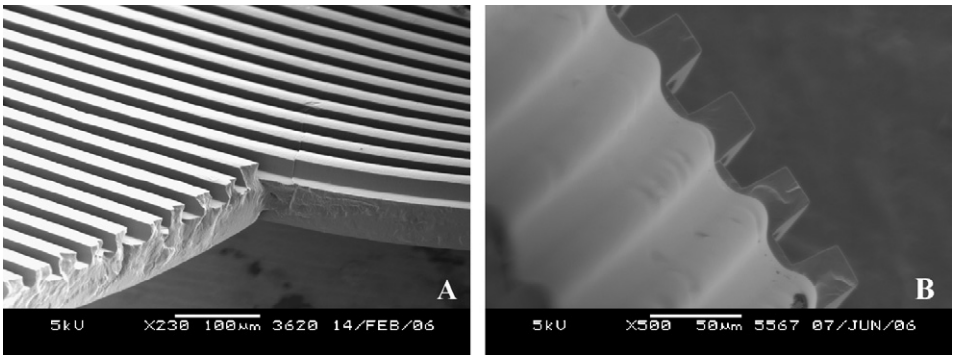

Fig. 3. SEM pictures of micro-patterned membranes: (A) cross-section/top surface with a thick (~50 μm) continuous film and (B) cross-section/bottom surface with a thin (~5 μm) continuous film.

through the thicker part and the flux through the thinner part of the membrane. Eq. (3) gives the theoretical advantage (T) of micro-patterning a membrane. J, D and Δc are, respectively, the flux, diffusion coefficient and concentration difference over a membrane of effective thickness Δx.

$$J_{\text{flat}}^{\text{theory}} = -D\frac{\Delta c}{\Delta x} \tag{1}$$

$$J_{\text{patterned}}^{\text{theory}} = \frac{30}{50}\left(-D\frac{\Delta c}{\Delta x + 10}\right) + \frac{20}{50}\left(-D\frac{\Delta c}{\Delta x - 15}\right) \tag{2}$$

$$T = \frac{J_{\text{patterned}}^{\text{theory}} - J_{\text{flat}}^{\text{theory}}}{J_{\text{flat}}^{\text{theory}}} \times 100 \tag{3}$$

Simulations were done to take the lateral gas diffusion into account that occurs in the micro-patterned membrane. Fig. 4 shows the concentration profile of gas permeating through a cross-section of the micro-patterned membrane. The diffusion coefficient was considered constant for this simulation. The concentration profile changes from high concentration (white) to zero concentration (black).

The effect of the micro-pattern on the concentration profile is clearly visible in this figure. Mass transfer through the thinner continuous film is faster than through the thicker ridges due to the increased concentration gradient. Compared to the analytical calculations, lateral transport enhances the average concentration in the ridge and thus diffusion through the ridges. The micro-patterned membrane can be compared to a composite membrane: a thin selective layer and a thicker pattern for mechanical stability.

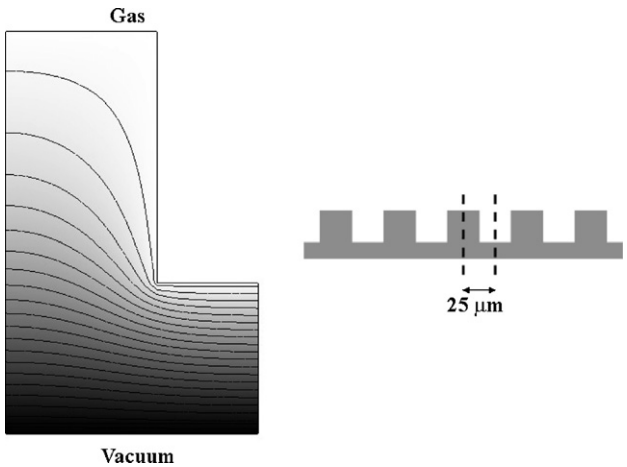

Fig. 4. Concentration profile (left) of gas diffusing through a section of a micro-patterned membrane (right).

Gas permeation measurements were performed to verify the theoretical expectations and simulation results. The flux of a micro-patterned membrane was normalized against its effective thickness (Eq. (4)). Eq. (5) gives the average permeability (P) of multiple flat membranes. These individual permeabilities are calculated the same way as in Eq. (4). The experimental advantage (E) of micro-patterning a membrane is calculated with Eq. (6).

$$P_{\text{patterned}}^{\text{exp}} = J_{\text{patterned}}^{\text{exp}}\,\Delta x \tag{4}$$

$$\left\langle P_{\text{flat}}^{\text{exp}} \right\rangle = \frac{P_{\text{flat},1}^{\text{exp}} + \cdots + P_{\text{flat},n}^{\text{exp}}}{n} \tag{5}$$

$$E = \frac{P_{\text{patterned}}^{\text{exp}} - \left\langle P_{\text{flat}}^{\text{exp}} \right\rangle}{\left\langle P_{\text{flat}}^{\text{exp}} \right\rangle} \times 100 \tag{6}$$

In Fig. 5 the flux enhancement is plotted versus the effective membrane thickness. The enhancement as calculated from simulations with a constant diffusion coefficient (●) is significantly stronger than for the analytical calculations (—). This is the sole effect of gas diffusing laterally through the micro-patterned membrane. The flux enhancement at high effective membrane thicknesses becomes less due to the fact that the height of the ridges is small compared to the total thickness of the membrane. Membrane (A) in Fig. 3, e.g., will benefit less from the micro-pattern compared to membrane (B). The theoretical minimum effective thickness for this geometry is 15 μm. At this thickness, all material is just enough to fill the mold valleys and no continuous film will be formed.

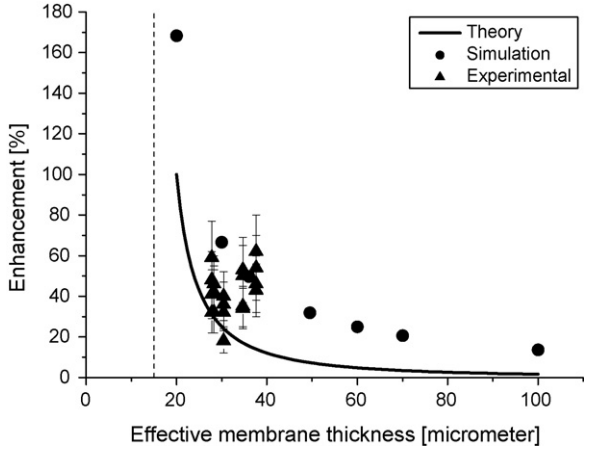

Fig. 5. Enhancement of gas permeation through micro-patterned membranes compared to flat membranes: (—) analytical calculations, (●) simulations and (▲) experimental results. The dashed line is the minimum effective thickness for the geometry which is studied.

Table 1
Raw gas permeability data per individual micro-patterned membrane and averaged for all flat membranes

Membrane	Δx (μm)	$J^{exp}\,\Delta x$ (N_2) (Barrer)	$J^{exp}\,\Delta x$ (He) (Barrer)	$J^{exp}\,\Delta x$ (O_2) (Barrer)	$J^{exp}\,\Delta x$ (CO_2) (Barrer)
Micro-patterned 1	27.8	22.8	53.2	43.8	265.9
Micro-patterned 2	28.8	20.8	47.4	47.0	266.1
Micro-patterned 3	30.4	18.8	49.0	46.2	223.0
Micro-patterned 4	34.7	19.2	48.1	49.6	288.4
Micro-patterned 5	37.6	20.4	52.4	50.7	304.4
Flat (average)	10.5–39.6	14.8 ± 1.8	36.0 ± 4.6	33.0 ± 4.3	188.4 ± 23.0

The experimental data (▲) was obtained from gas permeation measurements with different gases (N_2, He, O_2 and CO_2; measured in that order). Five thicknesses using four gases each were measured, resulting in 20 experimental points. Per point, the results of a series of flat membranes are compared to the results of a micro-patterned membrane. The error is large due to the fact that the reproducibility for different membranes was limited (standard deviation of 13%). The membrane thicknesses were measured from SEM pictures, which do not take local variations into account. Nevertheless, the experimental values still show that the advantage of micro-patterning membranes is significant. The theoretical and modeling trends are the same for all gases and concentrations. Due to the fact that only single gases were measured experimentally, concentration polarization is non-existent here.

The raw permeability data for calculating the experimental advantage is given in Table 1. The average selectivity of helium, oxygen and carbon dioxide over nitrogen are: $He/N_2 = 2.50 \pm 0.18$, $O_2/N_2 = 2.34 \pm 0.31$, $CO_2/N_2 = 13.37 \pm 2.13$. These selectivities were found for both flat and micro-patterned membranes. The measured selectivity O_2/N_2 corresponds to similar block copolymers in literature (2.3 at 308 K for TPE 416 [7] and 2.8 at 303 K for Kraton™ 1101 [8]). Other gas selectivities could not be found for this (type of) block copolymer.

3.3. Tensile stress

Tensile stress measurements were performed on flat and micro-patterned membranes to determine the mechanical strength. The micro-patterned membranes were measured both parallel (longitudinal) and perpendicular (transverse) to the line pattern. By micro-patterning with lines, the material becomes mechanically anisotropic: applying longitudinal strain yields higher tensile stresses than applying transverse strain. Straining a micro-patterned membrane on a 45° angle theoretically gives an average value between the longitudinal and transverse stress. This relationship can be compared to fiber-reinforced materials (Eq. (7)) [9].

$$\sigma(\theta) = \sigma_{\text{parallel}} \cos^2(\theta) + \sigma_{\text{perpendicular}} \sin^2(\theta) \quad (7)$$

Table 2 shows the average measured tensile stresses and their standard deviations per situation. When comparing flat membranes to micro-patterned membranes under longitudinal strain, one can conclude that micro-patterning results in a loss of stress of 28%. Theoretically it was expected to be 0%. At this moment we do not understand the reason for the loss of stress. A few possible explanations are discussed. The difference could originate from local variations in the thickness of the film. As the thickness is determined by SEM (a local technique), it is difficult to rule out variations. Another possibility could be differences in clamping the membranes into the set-up. The contact with the clamps on a micro-scale is different for a micro-patterned membrane compared to a flat membrane.

When applying transverse strain, the tensile stress is much lower than the stress for flat membranes (42% loss). A loss is expected as it is caused by a difference in stress-distribution. The stress during transverse strain is mostly located in the thin continuous film and not through the top part of the ridges.

The tensile stress for ridges under a 45° angle was also measured. According to Eq. (7) the theoretical stress at 45° should be in the middle between longitudinal and transverse straining (0.64 MPa). As seen from Table 2, the value is close to this theoretical value.

These losses in mechanical strength are comparable to the losses of a film that has been reduced in thickness to reach the same increase in flux. Due to its anisotropy, however, the line pattern does not yield the optimal structure when mechanical strength is concerned. The most promising micro-pattern would probably be one with a continuous matrix like a honeycomb well pattern.

Table 2
Results of tensile stress measurements on flat and micro-patterned membranes in different straining directions

Straining direction	Average σ at 5% strain (MPa)
Flat: all directions	0.98 ± 0.16
Micro-patterned: longitudinal	0.71 ± 0.08
Micro-patterned: 45° angle	0.61 ± 0.06
Micro-patterned: transverse	0.57 ± 0.04

3.4. Micro-patterning compared to composite membranes

When the pattern faces the permeate side, a micro-patterned membrane can also be seen as a continuous layer with a built-in (permeable) mechanical support. To verify if the micro-patterning is a good alternative for composite membranes, diffusive flux simulations are compared for both membranes (Fig. 6). All dimensions are similar to the ones in Fig. 2. The continuous layer has been varied from 5 to 85 μm.

A comparison of calculated diffusive fluxes through micro-patterned and composite membranes shows an enhancement for the micro-patterned membranes (Table 3). For a 5-μm-thick continuous layer, the flux of a completely permeable membrane is

Fig. 6. Schematic representation of the cross-section of a micro-patterned membrane (left) and a composite membrane (right) with the same dimensions.

Table 3
Calculations from simulations of the diffusive flux enhancement of a micro-patterned compared to a composite membrane

Thickness continuous layer (μm)	Enhancement (%)
5	38.2
15	31.1
21	24.0
34.5	16.2
45	14.7
55	12.0
85	8.2

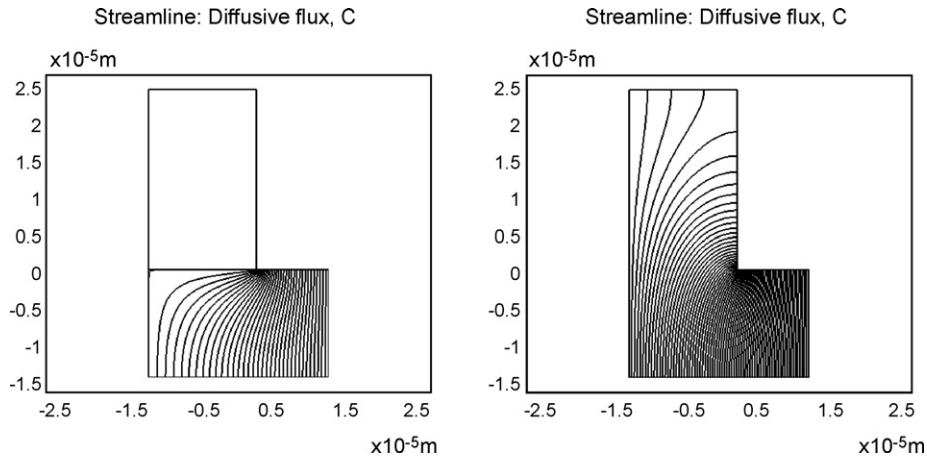

Fig. 7. Diffusive flux streamlines of (left) a composite membrane with a very low permeable support layer (here on top) and (right) a completely permeable micro-patterned membrane. Gas concentration is high at the bottom and low on top.

almost 40% higher. The calculation of the enhancement is similar to Eq. (3).

Fig. 7 shows the diffusive flux paths through both types of membranes. A rather simplified approach for calculating the effective diffusion length in a composite membrane is described by Eq. (8) [10]. This is a corrected version of the equation first published by Strathmann et al. [11,12]. It assumes a linear diffusion path from the furthest point to the pore (l_{max}). In this particular case the pore is the space between two ridges.

$$l_{eff} = \varepsilon l_0 + (1-\varepsilon)\frac{l_{max}+l_0}{2}$$
$$= \varepsilon l_0 + (1-\varepsilon)\frac{1}{2}\left[\sqrt{\left(r^2\frac{(1-\varepsilon)^2}{\varepsilon^2}+l_0^2\right)}+l_0\right] \quad (8)$$

Finite element simulations (Fig. 7) show that the assumption of a linear diffusion path is incorrect. The diffusive flux streamline from the furthest point to the pore in the composite membrane is strongly curved. This indicates that the decrease in diffusive flux for the composite membrane is even more for the simulations than in the theory proposed in literature. The comparison of effective diffusion lengths (l_{eff}) calculated from Eq. (8) and from the simulations supports this statement: a membrane with a 5-μm-thick continuous layer has a simulated diffusion path of 17.2 μm compared to 8.2 μm using Eq. (8). These results underline the importance of the lateral diffusion through the ridges. Therefore a micro-patterned membrane can (to some extent) be regarded as a composite membrane with a permeable support.

4. Conclusions

Micro-patterning one side of a flat membrane provides variations in thickness. Creating variations in diffusion paths through a dense gas permeation membrane has proven to increase overall gas permeation.

Experimental gas permeability results of patterned membranes were compared to non-patterned membranes with the same effective thicknesses. Four different gases (nitrogen, helium, oxygen and carbon dioxide) were used. Under the same conditions, the patterned membrane showed an increase in gas permeability. Analytical calculations predicted an increase in flux for the micro-patterned membranes. The lateral flux was included in finite element simulations, which resulted in an even stronger enhancement. The experimental values fluctuated between these two calculations. In all cases, the enhancement becomes larger for thinner membranes. Selectivity values did not depend on the structure of the membrane.

Thinner membranes have the disadvantage of becoming mechanically weaker. Micro-patterning limits the loss in mechanical strength by creating a geometry that is comparable to a composite membrane. Fluxes are enhanced significantly compared to the conventional composite membrane build-up if the support layer is of the same material as the separating layer. Due to its mechanical anisotropy the line pattern investigated in this paper is not the optimal structure in terms of membrane strength.

Although the experiments were performed with only one polymer and one pattern, micro-patterning is a general principle which is valid for all diffusion driven-processes.

Acknowledgements

This research is carried out within the framework of the micro- and nanofluidics spearhead of the University Twente. MicroNed is thanked for its financial support. The discussions on the tensile measurements with Ype van der Zijpp, Ton van den Boogaard and Erik van de Ven were also much appreciated.

Nomenclature

c_0	initial gas concentration (mol/m^3)
Δc	concentration difference over the membrane (g/cm^3)
D	diffusion coefficient (m^2/s)
E	experimental advantage of a micro-patterned membrane over a flat membrane (%)
$J^{exp}_{patterned}$	experimental flux through a micro-patterned membrane (GPU = gas permeation unit, 10^{-6} cm^3(STP) cm^{-2} s^{-1} cm Hg^{-1})
J^{theory}_{flat}	theoretical flux through a flat membrane (GPU = gas permeation unit, 10^{-6} cm^3(STP) cm^{-2} s^{-1} cm Hg^{-1})
$J^{theory}_{patterned}$	theoretical flux through a micro-patterned membrane (GPU = gas permeation unit, 10^{-6} cm^3(STP) cm^{-2} s^{-1} cm Hg^{-1})
l_{eff}	effective diffusion length through the selective layer of a composite membrane (m)

l_{max}	maximal linear diffusion path length through the selective layer to a pore (m)
l_0	thickness of the selective layer of a composite membrane(m)
n	number of values to average
$P^{exp}_{flat,n}$	experimental permeability of the nth flat membrane (Barrer, 10^{-10} cm^3(STP) cm cm^{-2} s^{-1} cm Hg^{-1})
$P^{exp}_{patterned}$	experimental permeability of a micro-patterned membrane (Barrer, 10^{-10} cm^3(STP) cm cm^{-2} s^{-1} cm Hg^{-1})
$\langle P^{exp}_{flat} \rangle$	average experimental permeability of all flat membranes (Barrer, 10^{-10} cm^3(STP) cm cm^{-2} s^{-1} cm Hg^{-1})
r	pore radius of the support layer of a composite membrane (m)
T	theoretical advantage of a micro-patterned membrane over a flat membrane (%)
Δx	effective membrane thickness (μm)

Greek symbols

ε	porosity of the support layer in a composite membrane (-)
θ	angle (°)
σ	tensile stress = force over the cross-sectional area (MPa)
$\sigma(\theta)$	tensile stress with fibers (ridges) on an angle θ (MPa)
$\sigma_{parallel}$	tensile stress parallel to the fibers (ridges) (MPa)
$\sigma_{perpendicular}$	tensile stress perpendicular to the fibers (ridges) (MPa)

References

[1] M. Ulbricht, Advanced functional polymer membranes, Polymer 47 (2006) 2217.
[2] A.M. Gronda, S. Buechel, E.L. Cussler, Mass transfer in corrugated membranes, J. Membr. Sci. 165 (2000) 177.
[3] W. Nijdam, J. de Jong, C.J.M. van Rijn, T. Visser, L. Versteeg, G. Kapantaidakis, G.H. Koops, M. Wessling, High performance micro-engineered hollow fiber membranes by smart spinneret design, J. Membr. Sci. 256 (2005) 209.
[4] L. Vogelaar, R.G.H. Lammertink, J.N. Barsema, W. Nijdam, L.A.M. Bolhuis-Versteeg, C.J.M. van Rijn, M. Wessling, Phase separation micromolding: a new generic approach for microstructuring various materials, Small 1 (2005) 645.
[5] A. Bos, High pressure CO_2/CH_4 separation with glassy polymer membranes—aspects of CO_2-induced plasticization, PhD thesis, University of Twente, 1996, p. 144.
[6] S.C. George, S. Thomas, Transport phenomena through polymeric systems, Prog. Polym. Sci. 26 (2001) 985.
[7] J.M. Yang, C.P.C. Chian, K.Y. Hsu, Oxygen permeation in SBS-g-DMAEMA copolymer membrane prepared by UV photografting without degassing, J. Membr. Sci. 153 (1999) 175.
[8] G.H. Hsiue, J.S. Yang, Polymeric complex membranes based on styrene–diene–styrene triblock copolymers for oxygen enrichment, Polym. Adv. Technol. 7 (1996) 686.
[9] K.H.G. Ashbee, Fundamental Principles of Fiber Reinforced Composites, 1st ed., Technomic Publishing Company Inc., Lancaster, 1989.
[10] K.-V. Peinemann, Composite and Mixed Matrix Membranes, XXI EMS Summer School, Geesthacht, Germany, 2004.
[11] H. Strathmann, C.M. Bell, W. Gudernatsch, K. Kimmerle, Development of solvent-selective membranes and their use in gas separation and pervaporation, Chem. Ing. Tech. 60 (1988) 590.
[12] H. Strathmann, C.M. Bell, J. Kerres, Gas separation and pervaporation—membrane and module development, Desalination 77 (1990) 259.